文章编号：1000-8608(2018)04-0331-11

Encapsulation of Co metal by nitrogen doped porous carbon for catalytic removal of organic pollutants

WANG Guanlong, BI Chenxi, CHEN Shuo*, QUAN Xie, YU Hongtao

(Key Laboratory of Industrial Ecology and Environmental Engineering, MOE, Dalian University of Technology, Dalian 116024, China)

Abstract: Sulfate radical ($SO_4^{\cdot -}$), which is usually obtained by peroxymonosulfate (PMS) activation, has attracted much interest in the research of organic pollutant degradation for its high oxidative capability. Herein, a Co@nitrogen doped porous carbon (Co@NPC) core-shell catalyst is prepared using ZIF-67 as the precursor by two-step heating treatment. Different carbonization temperatures are chosen to tune the structure and composition of carbon shell, and its relationship with catalytic performance is investigated. The results show that the mesopore volume and the carbon shell thickness increase gradually with the increase of carbonization temperature, while the catalytic performance is enhanced with the increasing ratio of mesopore volume to carbon shell thickness. The Co@NPC carbonized at 850 ℃ performs best for phenol degradation, whose kinetic constant for phenol degradation is 110.8 times higher than that of heterogeneous Co_3O_4 and even 4.6 times higher than that of the reported optimum homogeneous Co^{2+} for PMS activation. Moreover, the Co@NPC displays good stability and obvious reduction of Co leaching when the number of carbon layer is higher than 3. The mesopore volume and thickness of carbon shell play significant roles in the PMS activation, while the content of graphitic N could also influence the catalytic performance.

Key words: peroxymonosulfate (PMS); sulfate radical; nitrogen doped porous carbon; core-shell catalyst; phenol degradation

0 Introduction

Sulfate radical ($SO_4^{\cdot -}$) based advanced oxidation process (AOP) has become an attractive alternative to the hydroxyl radical (·OH) based AOP for environmental remediation, owing to its advantages such as high redox potential (2.5-3.2 V), long radical lifetime (20-30 μs) and wide pH adaption (2-8)[1-2]. Commonly, $SO_4^{\cdot -}$ could be generated from activating peroxymonosulfate (PMS) via UV irradiation[3], thermal activation[4] and transition metal or metal oxide catalysis[5-6]. Because the transition metal catalysis enables effective activation of PMS and needs no energy

Received by: 2017-12-10; **Revised by**: 2018-05-25.
Supported by: National Natural Science Foundation of China (Major Project: No. 21590813); Program of Introducing Talents of Discipline to Universities (B13012).
Corresponding authors: WANG Guanlong (1990-), Male, Doc., E-mail: stevewgl@mail.dlut.edu.cn; CHEN Shuo* (1974-), Female, Doc., Associa. Prof., E-mail: shuochen@dlut.edu.cn.

addition, this process received more research interest. In particular, the Co based catalysts have been found the best PMS activator in this system. However, the homogeneous Co catalysis process suffers from the toxic Co ions discharge and difficult catalysts recycle[7-8]. The heterogeneous Co-based catalysts could alleviate these drawbacks, but they usually exhibit low catalytic efficiency resulting from the metal aggregation and reduced mass transfer[9]. Moreover, the Co leaching of heterogeneous metal catalysts remains serious due to the instability of Co-based catalysts in aqueous solution, inducing the adverse effect to environment. Therefore, it is highly desirable to design a novel, effective and stable PMS catalyst.

Encapsulating the Co nanoparticles into a porous shell to form a core-shell structure may alleviate the above problems[9]. On the one hand, the porous shell could impede the aggregation and leaching of Co nanoparticles, and protect the inside Co nanoparticles from outside harsh environment[10]. On the other hand, the porous structure facilitates the transport of reactant and products[11]. Zeng, *et al*.[9] constructed a yolk-shell Co_3O_4@metal-organic frameworks (MOFs) catalyst for PMS activation, for which the degradation efficiency of 4-CP reached almost 100% within 60 min compared to only 59.6% under the same conditions for bare Co_3O_4 nanoparticles. However, in that work the MOFs shell showed no catalytic activity. The catalytic efficiency of core-shell catalyst would be largely improved if both core and shell could serve as the active sites for PMS activation.

Carbon materials are believed to be ideal materials for constructing the shell of core-shell catalysts due to its large surface area, good chemical stability and low cost[12]. Especially, the intrinsic catalytic capability of carbon materials makes it possible for them to participate the catalytic reaction[13]. Recently, the carbon materials such as activate carbon, graphene and porous carbon have shown their capability in PMS activation. Moreover, the heteroatom doping method such as the nitrogen doping was found to further enhance the catalytic efficiency of carbon towards PMS because the nitrogen with higher electronegativity than carbon could induce high positive charge on carbon and effectively activate it, thus promoting the adsorption and activation of negatively charged PMS on carbon[14-15].

Inspired by it, constructing a core-shell catalyst with nitrogen doped porous carbon as the shell and Co nanoparticles as the core may form a highly efficient and stable catalyst for PMS activation. The Co encapsulated by nitrogen doped porous carbon possesses several advantages in PMS activation: (1) It was reported the interactions between Co core and carbon-shell could reduce the work function of carbon shell and enhance its electron-donating capability in the Co @ carbon core-shell structure[16]. Hence, the doped nitrogen and encapsulated Co may synergistically modify the electronic structure of carbon and enhance the catalytic activity of carbon, which is beneficial for the enhanced PMS activation on carbon. (2) The porous carbon shell is favorable for the transport of the PMS and products. (3) The porous carbon shell protects the Co from aggregation and leaching, improving the stability of catalysts[17]. To realize high PMS catalytic efficiency on this core-shell catalyst, it is critical to rationally design and regulate the carbon shell. The thin carbon shell is favorable for the mass transfer and the interaction between carbon shell and Co core, while the thick carbon shell could alleviate the metal leaching. However, facile and effective regulation over the shell structure during the development of the core-shell catalyst remains a challenge.

The metal-organic frameworks (MOFs), composed of metal cluster and various organic ligands, are ideal precursors to construct the metal @ carbon nanostructure through the carbonization treatment[18-19]. Moreover, the carbon shell thickness and composition could be

controlled via controlling the carbonization process and temperature[20-21]. In this work, the ZIF-67, a MOF rich in Co and N (Co content: 25.8%, N content: 26.7%), was used as the template to construct the Co@nitrogen doped porous carbon (Co@NPC). Different carbonization temperature (750 ℃, 850 ℃ and 950 ℃) were chosen to prepare the carbon shell with different structures and compositions. The phenol, bisphenol A and rhodamine B were used to evaluate the catalytic performance of Co@NPC for PMS activation and the effect of carbon structure and composition on catalytic performance was studied. Furthermore, the possible catalytic mechanism was explored.

1 Experiment

1.1 Preparation of ZIF-67

The typical preparation process of ZIF-67 was as follows. Solution A: 2.25 g $Co(NO_3)_2 \cdot 6H_2O$ was dissolved in 15 mL ultrapure water. Solution B: 27.5 g 2-methylimidazole was dissolved in 100 mL ultrapure water. Then the solution A was slowly added into the solution B and stirred for 6 h. The catalysts were obtained through centrifuging at 8 000 r/min for 10 min. The resulting catalysts were then washed with methanol and ultrapure water respectively, and finally dried at 50 ℃ in oven.

1.2 Preparation of Co@NPC

Co@NPC was prepared through carbonization of ZIF-67. Typically, for the preparation of Co@NPC, the powder of ZIF-67 was heated to 450 ℃ (5 ℃ · min^{-1}) in a tube furnace under Ar gas flow, and maintained at this temperature for 2 h. This process involved the collapse of the framework and the formation of new component. Then the temperature is elevated to 750 ℃, 850 ℃ and 950 ℃ respectively and maintained at it for 1 h to realize the catalytic graphitization by Co metal. This two-step calcination resulted in the final Co@NPC core-shell catalyst. For convenient description, the Co@NPC carbonized at 750 ℃, 850 ℃ and 950 ℃ were denoted as Co@NPC-750, Co@NPC-850 and Co@NPC-950.

1.3 Characterization

The morphologies of catalysts were revealed by field emission scanning electron microscope (Hitachi S-4800, FE-SEM) and transmission electron microscopy (FEI-Tecnai $G^2$20, TEM). The structure properties of the catalysts including the crystal structure and carbonization degree were performed by X-ray diffraction (Shimadzu LabX XRD-6000, XRD) and Raman spectrum (Renishaw Micro-Raman System 2000 Spectrometer). The pore structure and specific surface area of catalysts were determined through N_2 adsorption-desorption isotherms at 77 K with a Quadrasorb instrument. The Co content was measured by ICP-AES (Optima 2000 DV). The element composition and species distribution were characterized by X-ray photoelectron spectroscopy (XPS) got from a VG ESCALAB 250 spectrometer using a non monochromatized AlKα X-ray source (1 486.6 eV).

1.4 Evaluation of catalytic performance

The catalytic performance of catalysts was evaluated through pollutant removal. Initially, 2.5 mg Co@NPC catalyst was dispersed in 50 mL solution containing 20 mg · L^{-1} phenol. Phosphate buffer (1 mmol · L^{-1}, pH 7) was added into the solution to maintain the pH at 7. The solution was stirred to reach the adsorption-desorption equilibrium, and then 1.6 mmol · L^{-1} PMS was added to initiate the reaction. 1 mL solution was withdrawn at the given time and filtered through a 0.22 μm millipore film for further analysis. 0.1 mL methanol was immediately injected into the reaction solution for scavenging the residual radicals. The effects of catalyst dosage, PMS loading and pH on degradation efficiency of phenol were evaluated. The pH of solution was adjusted by adding 0.1 mmol · L^{-1} HCl or NaOH. In the reusability test of catalyst, the used Co@NPC was collected via vacuum filtration and washed with ultrapure water (resistivity is bigger than 18 MΩ · cm).

1.5 Analytic methods

The concentrations of phenol and bisphenol A (BPA) were analyzed by a high performance

liquid chromatography (HPLC, Waters). The mobile phase was 30% methanol and 70% ultrapure water at a flow rate of 1 mL · min^{-1}. The organics were separated by a C-18 column and determined by a PDA detector. TOC concentration of aliquot samples was determined using a total carbon analyzer (Shimadzu TOC-VCPH, Japan). The concentration of rhodamine B (RhB) was measured by a UV-vis spectrometer at λ=552 nm.

2 Results and discussion

2.1 The characteristics of Co@NPC

The morphologies of ZIF-67 and Co@NPC were characterized using SEM and TEM. As shown in Fig. 1, SEM images of ZIF-67 and Co@NPC-850 illustrate the similar polyhedral structure, indicating the carbonization process does not destroy the structure of the original morphology of ZIF-67. The average size of ZIF-67 is around 300 nm, yet reduced to around 100 nm for Co@NPC-850, which is possibly owing to the changes of the precursor structure and the loss of oxygen containing groups during the carbonization process. TEM images further show the microstructure of Co@NPC carbonized at different temperatures (Fig. 2). It is found that the Co nanoparticle with a lattice fringe of 0.208 nm is completely encapsulated by carbon cages in 3-10 layers. The lattice fringe of carbon layers is 0.342 nm, which is assigned to (002) plane of graphene. These results suggest that the as-synthesized Co@NPC samples demonstrate a core-shell structure and retain a highly ordered structure of graphitic structure. The carbon layers of Co@NPC-750, Co@NPC-850 and Co@NPC-950 are 3, 5 and 8, respectively. The Co nanoparticles in Co@NPC-950 could not be clearly observed on TEM images because they are completely encapsulated by relatively thick carbon layers. These results reveal that the thickness of graphitic carbon increases with the increasing carbonization temperatures and thereafter contributes to an increased carbon layers.

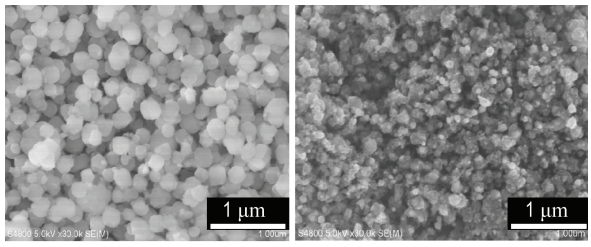

(a) ZIF-67 (b) Co@NPC-850

Fig. 1 The SEM images of ZIF-67 and Co@NPC-850

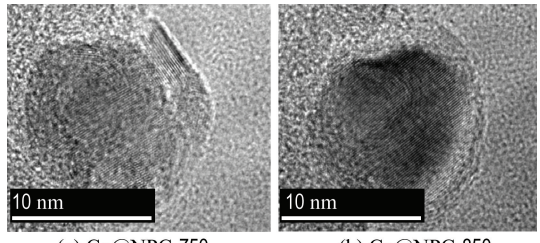

(a) Co@NPC-750 (b) Co@NPC-850

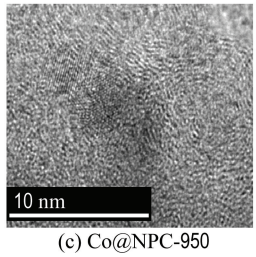

(c) Co@NPC-950

Fig. 2 The TEM images of Co@NPC

Raman analysis was also carried out to get structural information of Co@NPC. As shown in Fig. 3(a), the characteristic D band (defect carbon structure) and G band (graphitized carbon structure) appear at 1 360 cm^{-1} and 1 580 cm^{-1}, respectively. The relative intensity of the D and G peaks (I_D/I_G) of Co@NPC decreases with the increment of carbonization temperatures, suggesting the higher carbonization temperature results in better graphitization degree. Furthermore, XPS measurements were conducted to reveal the element composition of Co@NPC. As shown in Fig. 3(b), the characteristic peaks of Co, N and C are clearly observed on all Co@NPC samples, illustrating both Co and N are successfully doped into carbon lattice. Moreover, the Co and N contents gradually decrease with the increase of carbonization temperature (Tab. 1), which is ascribed to the growing thick carbon layers and the loss of N-containing groups.

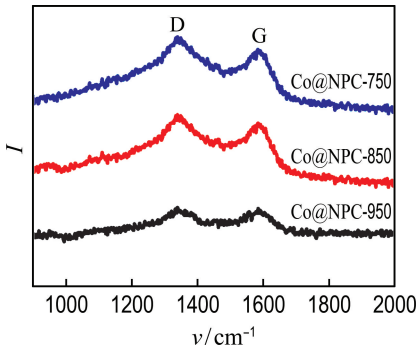

(a) Raman spectra

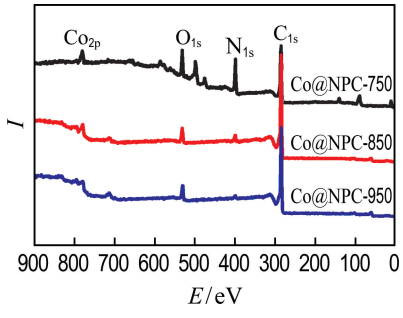

(b) XPS spectra

Fig. 3 Raman spectra and XPS spectra of Co@NPC-750, Co@NPC-850 and Co@NPC-950

Tab. 1 Element composition of Co@NPC

Sample	Atomic mass fraction / %			
	C	N	O	Co
Co@NPC-750	64.57	22.68	11.68	1.07
Co@NPC-850	87.82	4.54	6.67	0.97
Co@NPC-950	88.36	3.25	7.71	0.68

2.2 The catalytic performance of Co@NPC

The catalytic performance of Co@NPC for PMS activation was evaluated using phenol as the model pollutant. For comparison, the homogeneous Co^{2+} and heterogeneous Co_3O_4 were employed as references. Fig. 4(a) shows that almost no phenol is removed by PMS alone after 60 min, meaning the PMS itself could hardly oxidize the phenol. Less than 10% phenol is removed when only the catalysts are added into the solution, which is probably attributed to the adsorption of phenol on catalyst. After the addition of PMS, the phenol concentration rapidly decreases. The Co@NPC-850/PMS performs best with almost complete removal (about 100%) of phenol within 15 min, followed by the Co@NPC-950/PMS and Co@NPC-750/PMS, which could almost completely remove phenol within 30 min and 60 min, respectively. Under the same catalyst dosage, the Co@NPC-850/PMS performs better than heterogeneous Co_3O_4/PMS which removes only 30% phenol within 40 min, and even outperforms the homogeneous Co^{2+}/PMS (the most effective PMS catalytic system) which removes about 100% phenol within 40 min.

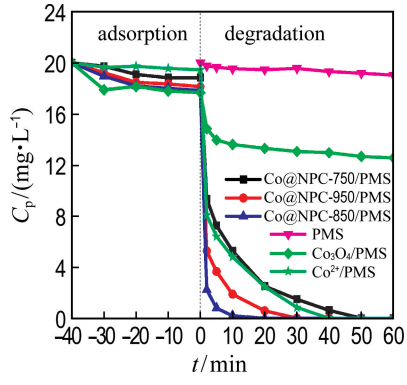

(a) PMS activation by Co@NPC

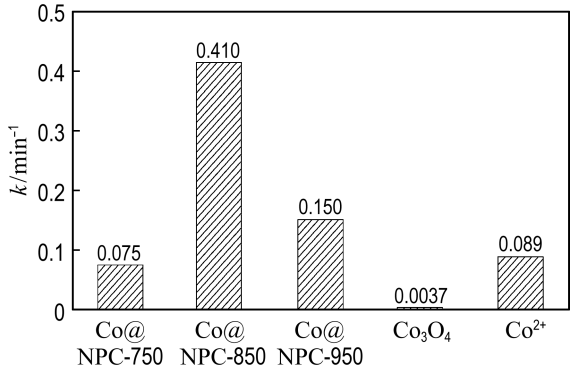

(b) Kinetic constant

Fig. 4 Catalytic performance for phenol degradation (C_{cat} = 0.05 g·L^{-1}, c_{PMS} = 1.6 mmol·L^{-1}, C_{poll} = 20 mg·L^{-1}, θ = 25 ℃, initial pH = 7.0)

The degradation process of phenol by Co@NPC/PMS is fitted well with the pseudo-first-order reaction. As shown in Fig. 4(b), the kinetic constants of phenol oxidation on Co@NPC-750, Co@NPC-850, Co@NPC-950, homogeneous Co^{2+} and heterogeneous Co_3O_4 are 0.075 min^{-1}, 0.410 min^{-1}, 0.150 min^{-1}, 0.089 min^{-1} and 0.003 7 min^{-1}, respectively. The Co@NPC-850 shows best performance for PMS activation, whose catalytic efficiency for phenol

degradation is 4.6 times and 110.8 times that of homogeneous Co^{2+} and heterogeneous Co_3O_4, respectively.

Other recalcitrant pollutants including BPA and RhB were also selected to evaluate the catalytic performance of Co@NPC (Fig. 5). The results show that nearly 100% BPA and RhB are removed by Co@NPC/PMS within 30 min. The kinetic constants for the degradation of phenol, BPA and RhB reach 0.41 min^{-1}, 0.87 min^{-1} and 0.16 min^{-1}, respectively. It indicates that the Co@NPC/PMS system is capable of removing various refractory organic pollutants.

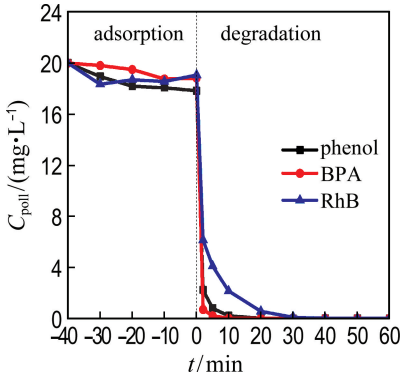

(a) Co@NPC/PMS system

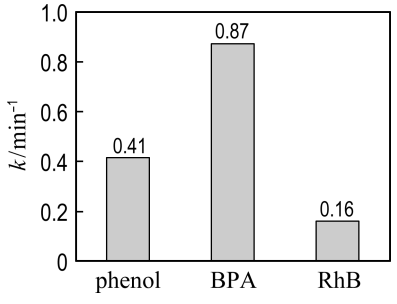

(b) Kinetic constant

Fig. 5 Catalytic performance for degradation of different pollutants (C_{cat} = 0.05 g·L^{-1}, c_{PMS} = 1.6 mmol·L^{-1}, C_{poll} = 20 mg·L^{-1}, θ = 25 ℃, initial pH = 7.0)

2.3 The effects of catalyst dosage, PMS concentration and pH on the catalytic performance of Co@NPC

As shown in Fig. 6(a), the phenol degradation efficiency is enhanced with the increase of catalyst concentration. Fig. 6(a) shows that the kinetic constant of Co@NPC for phenol degradation increases from 0.071 min^{-1} at 0.01 g·L^{-1} catalyst dosage to 1.00 min^{-1} at 0.10 g·L^{-1} catalyst dosage. The higher catalyst concentration could provide more active sites for radical generation, thus leading to better catalytic performance.

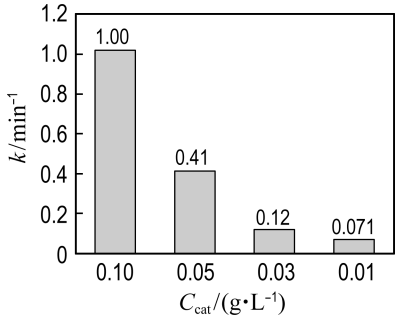

(a) Catalyst dosage

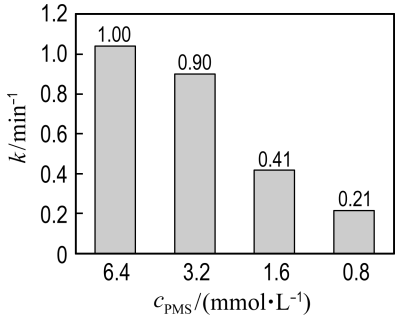

(b) PMS concentration

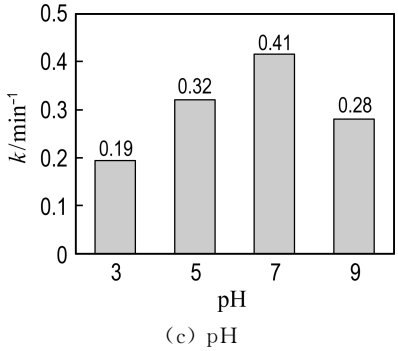

(c) pH

Fig. 6 The effects of conditions on phenol degradation

Similarly, higher PMS dosage also contributes to higher catalytic efficiency (Fig. 6(b)). The kinetic constant increases from 0.21 min^{-1} to 0.90 min^{-1} when the PMS dosage increases from 0.8 mmol·L^{-1} to 3.2 mmol·L^{-1}. However, only a slight increase of kinetic constant (from 0.90 min^{-1} to 1.00 min^{-1}) is observed when the PMS dosage

further increases to 6.4 mmol·L^{-1}. It is known the $SO_4^{\cdot-}$ or ·OH would be quenched by excess PMS (Eq. (1) and (2))[15], the slight increase of degradation efficiency may be ascribed to this quenching effect.

$$SO_4^{\cdot-} + HSO_5^- \longrightarrow SO_5^{\cdot-} + SO_4^{2-} + H^+ \quad (1)$$

$$\cdot OH + HSO_5^- \longrightarrow SO_5^{\cdot-} + H_2O \quad (2)$$

Fig. 6(c) shows that the Co@NPC/PMS system exhibits effective degradation of phenol over a wide pH range (3-9), which lies in the pH range of the natural water and wastewater. The kinetic constant of phenol degradation increases from 0.19 min^{-1} at pH=3 to 0.41 min^{-1} at pH=7, but then slightly decreases to 0.28 min^{-1} at pH=9. According to the pK_a of PMS ($pK_{a1}<0$ and $pK_{a2}=9.4$), PMS mainly exists as HSO_5^- when pH ranges from 3 to 7. In acidic condition, the H^+ prefers to bind with the O—O group of HSO_5^- via the H-bond binding. The electrostatic repulsion between HSO_5^- and the positively charged surface of Co@NPC (pH_{pzc} is around 7.2) causes the decreased catalytic efficiency. At the pH of 9.6, the phenol degradation efficiency decreases due to the self-decomposition of HSO_5^-.

2.4 The reusability and stability of Co@NPC

The reusability of Co@NPC catalysts for phenol degradation is presented in Fig. 7(a). The repetition use causes almost no decline of the catalytic activity of Co@NPC for phenol degradation, suggesting the good reusability of Co@NPC. To further evaluate the stability of Co@NPC, the Co leaching in each reaction cycle was detected. Fig. 7(b) shows that the Co leaching of Co@NPC/PMS system decreases gradually from 0.25 mg·L^{-1} in the 1st run to 0.01 mg·L^{-1} in the 5th run. This value is much lower than the National Standard for Co Discharge (GB 25467-2010, 1 mg·L^{-1}). The low Co leaching of Co@NPC may be ascribed to the protective effect of carbon shell. Fig. 7(c) shows the Co leaching of the Co@NPC carbonized at different temperatures. It could be found the Co leaching obviously decreases when the carbonization temperature increases from 750 ℃ to 850 ℃. The Co leaching reaches 1.03 mg·L^{-1}, 0.25 mg·L^{-1} and 0.08 mg·L^{-1} for the Co@NPC carbonized at 750 ℃, 850 ℃ and 950 ℃, respectively. The Co leaching is largely reduced when the carbon layer is more than 3.

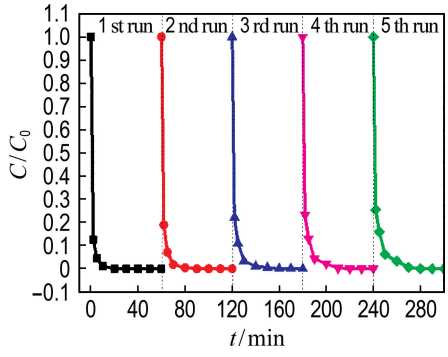

(a) The reusability of Co@NPC

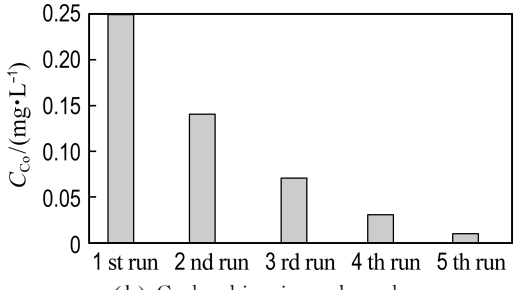

(b) Co leaching in each cycle

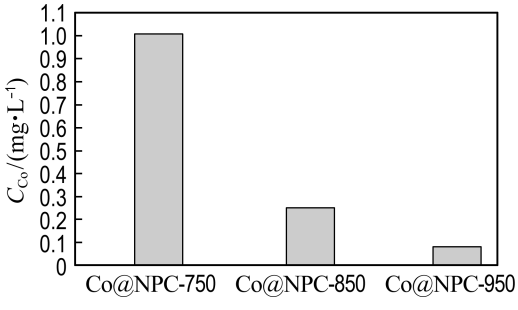

(c) Co leaching of different Co@NPC

Fig. 7 The reusability of Co@NPC for phenol degradation as a function of time, Co leaching in each cycle and different Co@NPC

2.5 The contribution of radicals in Co@NPC/PMS system

In order to disclose the radical formation in Co@NPC/PMS system, the radical quenching experiments were conducted. It is widely accepted that the alcohols with an α hydrogen such as methanol could readily react with both ·OH and $SO_4^{\cdot-}$ radicals. Alcohols without an α

hydrogen, such as tert-butyl alcohol (TBA), are also readily reactive toward •OH, but their reaction with $SO_4^{\cdot -}$ is over 1000-fold slower[10]. Thus, methanol and TBA were usually used to differentiate $SO_4^{\cdot -}$ from •OH. Fig. 8(a) shows slight decrease of phenol removal when TBA is added in the reaction system, and the reaction rate of phenol degradation decreases slightly from 0.41 min^{-1} (with no quencher) to 0.35 min^{-1} at a TBA and PMS mass ratio of 1 000 (Fig. 8(b)), implying almost no •OH is present in the Co@NPC/PMS system. In comparison, significant decrease of phenol removal could be observed when different concentrations of methanol were added (Fig. 8(a)). The reaction rate of phenol degradation decreases dramatically to 0.004 3 min^{-1} at a MeOH and PMS mass ratio of 1 000, indicating the $SO_4^{\cdot -}$ is the primary reactive species in catalytic system (Fig. 8(b)). Notably, still 40% phenol degradation is achieved after MeOH quenching, which suggests the existence of non-radical pathway in the catalytic system. As reported in previous researches, the non-radical mechanism refers to the process that the Co-N-PC serves as the mediator to conduct the electron transfer from target compound to PMS, leading to the oxidation of target compound without generating radicals[22].

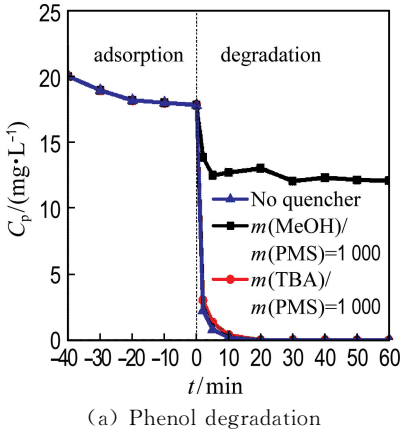

(a) Phenol degradation

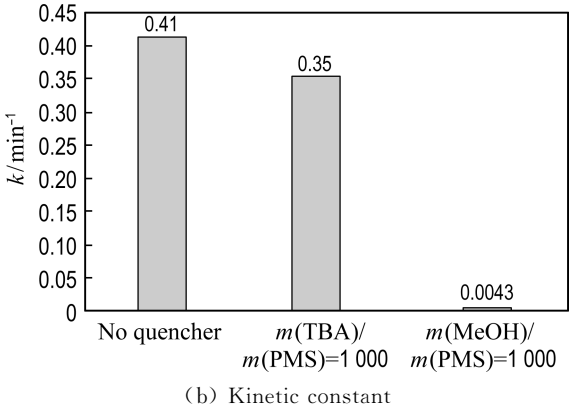

(b) Kinetic constant

Fig. 8 Phenol degradation as a function of time and kinetic constant of phenol degradation with the addition of TBA and MeOH

2.6 The possible catalytic mechanism of Co@NPC

It is generally accepted that the catalyst with high specific surface area is favorable for the catalytic reactions because it can offer abundant catalytic sites. For Co@NPC, their specific surface area follows the order of Co@NPC-950 > Co@NPC-850 > Co@NPC-750 (Tab. 2), whereas their reaction rate follows another order of Co@NPC-850 > Co@NPC-950 > Co@NPC-750. This result suggests the surface area of Co@NPC catalyst is not the primary factor responsible for its catalytic behavior, and other factors may dominate the performance of catalysts. Moreover, it is noted the mesopore volume of Co@NPC increases gradually with the increase of carbonization temperature. The higher mesopore volume is beneficial for the reactant transport.

Tab. 2 BET value, total pore volume and mesopore volume of Co@NPC

Sample	BET/ ($m^2 \cdot g^{-1}$)	Total pore volume/ ($cm^3 \cdot g^{-1}$)	Mesopore volume/ ($cm^3 \cdot g^{-1}$)
Co@NPC-750	183	0.22	0.18
Co@NPC-850	294	0.54	0.46
Co@NPC-950	365	0.68	0.55

As reported in previous work, the graphitic N may greatly influence the catalytic activity of N doped carbon in PMS activation[21]. To check the possible influence of graphitic N, the XPS spectra were performed to investigate the N species of Co@NPC. The four peaks corresponding to graphitic-N (401.1 eV), pyridinic-N (398.5

eV), pyrrolic-N (400.5 eV) and Co-N coordination site (Co-N_x) (399.2 eV)[23] respectively are present in each Co@NPC. The content of N species in different Co@NPC was summarized in Tab. 3, which was calculated from the total N content and their respective proportion. Tab. 3 shows that the Co@NPC-750 possesses higher graphitic N content than that of Co@NPC-950, but its catalytic activity is poorer. The results demonstrate the graphitic N is not the critical factor for PMS activation. In addition, the occurrence of Co-N_x suggests the Co core could produce the influence on the carbon shell, whereas with the increase of carbonization temperature, the Co-N_x content decreases gradually, suggesting the thicker carbon shell restricts the interaction between Co and carbon.

Tab. 3 Content of different N species in Co@NPC

Sample	Atomic mass fraction/%			
	Graphitic-N	Pyridinic-N	Co-N_x	Pyrrolic-N
Co@NPC-750	1.07	3.22	10.20	8.28
Co@NPC-850	1.23	1.17	1.08	1.05
Co@NPC-950	0.85	0.73	0.62	1.05

According to the result of Raman spectra, the graphitization degree of Co@NPC is enhanced with the increase of carbonization temperature. The enhanced graphitization degree means more sp^2 hybridized carbon structure is present in the carbon shell, and the sp^2 hybridized carbon structure could provide plentiful free-flowing π electrons for the electron transfer reaction. Moreover, the high graphitization degree is favorable for forming the thick carbon layers which inhibit the metal leaching. In this work, the Co@NPC-850 and Co@NPC-950 exhibits higher graphitization degree than Co@NPC-750, and the metal leaching of instable Co@NPC-750 is much higher than that of Co@NPC-850 and Co@NPC-950 (Fig. 9), leading to the higher catalytic activity of Co@NPC-850 and Co@NPC-950 than that of Co@NPC-750. Besides, the Co@NPC-850 and Co@NPC-950 possess higher mesopore volume than that of Co@NPC-750, which is beneficial for reactant transfer to the surface of catalyst.

Interestingly, although the Co@NPC-950 displays higher graphitization degree and mesopore volume than Co@NPC-850, the catalytic activity of Co@NPC-950 is still inferior to that of Co@NPC-850. This phenomenon may be explained by two possible reasons: Firstly, as shown in Tab. 3, the Co@NPC-850 possesses higher graphitic N content. Secondly, the TEM results indicate that the carbon layer of Co@NPC-950 is thicker than that of Co@NPC-850. Although the thick graphitic carbon layer can protect the Co from leaching, it enhances the resistance for reactant transfer and weakenes the interaction between Co core and carbon shell, thus resulting in the poorer catalytic performance of Co@NPC-950 than that of Co@NPC-850.

For better understanding the relationship between the structure of carbon shell and the catalytic activity of Co@NPC, the ratio of mesopore volume to carbon shell thickness for different Co@NPC was calculated. As shown in Fig. 9, the catalytic activity of Co@NPC is significantly enhanced with the increase of the ratio of mesopore volume to carbon shell thickness. This result confirms that the mesopore volume and the carbon shell thickness play important role in the catalytic performance of Co@NPC for PMS activation.

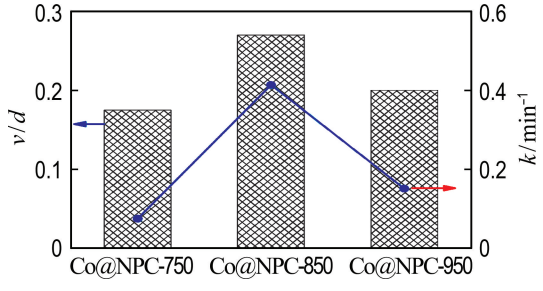

Fig. 9 The relationship between the value of mesopore volume/carbon shell thickness (v/d) and the kinetic constant for phenol degradation on Co@NPC

3 Conclusion

Two-step heating treatment was employed for preparing the Co@NPC core-shell catalysts. The Co@NPC displays significantly enhanced catalytic activity with the increase of the ratio between mesopore volume and carbon shell thickness. The kinetic constant of the best Co@NPC is 4.6 times higher than that of homogeneous Co^{2+} and 110.8 times higher than that of Co_3O_4. The Co@NPC also displays good stability in phenol degradation and less Co leaching (less than 0.25 mg · L^{-1}). Sulfate radical is the main reactive radical present in the Co@NPC/PMS system responsible for the pollutant degradation. The mesopore volume and carbon shell thickness play key role in Co@NPC for PMS activation, while the graphitic N content also influences the catalytic performance.

References:

[1] OH W D, DONG Z, LIM T T. Generation of sulfate radical through heterogeneous catalysis for organic contaminants removal: current development, challenges and prospects [J]. **Applied Catalysis B: Environmental**, 2016, **194**: 169-201.

[2] DENG Y, EZYSKE C M. Sulfate radical-advanced oxidation process (SR-AOP) for simultaneous removal of refractory organic contaminants and ammonia in landfill leachate [J]. **Water Research**, 2011, **45**(18): 6189-6194.

[3] LAU T K, CHU W, GRAHAM N J D. The aqueous degradation of butylated hydroxyanisole by $UV/S_2O_8^{2-}$: study of reaction mechanisms via dimerization and mineralization [J]. **Environmental Science & Technology**, 2007, **41**(2): 613-619.

[4] WALDEMER R H, TRATNYEK P G, JOHNSON R L, *et al*. Oxidation of chlorinated ethenes by heat-activated persulfate: Kinetics and products [J]. **Environmental Science & Technology**, 2007, **41**(3): 1010-1015.

[5] HU Peidong, LONG Mingce. Cobalt-catalyzed sulfate radical-based advanced oxidation: A review on heterogeneous catalysts and applications [J]. **Applied Catalysis B: Environmental**, 2016, **181**: 103-117.

[6] SHI Penghui, SU Ruijing, WAN Fengzhi, *et al*. Co_3O_4 nanocrystals on graphene oxide as a synergistic catalyst for degradation of Orange Ⅱ in water by advanced oxidation technology based on sulfate radicals [J]. **Applied Catalysis B: Environmental**, 2012, **123-124**: 265-272.

[7] FENG Yong, WU Deli, DENG Yu, *et al*. Sulfate radical-mediated degradation of sulfadiazine by $CuFeO_2$ rhombohedral crystal-catalyzed peroxymonosulfate: synergistic effects and mechanisms [J]. **Environmental Science & Technology**, 2016, **50**(6): 3119-3127.

[8] ZOU Jing, MA Jun, CHEN Liwei, *et al*. Rapid acceleration of ferrous iron/peroxymonosulfate oxidation of organic pollutants by promoting Fe(Ⅲ)/Fe(Ⅱ) cycle with hydroxylamine [J]. **Environmental Science & Technology**, 2013, **47**(20): 11685-11691.

[9] ZENG Tao, ZHANG Xiaole, WANG Saihua, *et al*. Spatial confinement of a Co_3O_4 catalyst in hollow metal-organic frameworks as a nanoreactor for improved degradation of organic pollutants [J]. **Environmental Science & Technology**, 2015, **49**(4): 2350-2357.

[10] LU Jia, ZHOU Weijia, WANG Likai, *et al*. Core-shell nanocomposites based on gold nanoparticle@zinc-iron-embedded porous carbons derived from metal-organic frameworks as efficient dual catalysts for oxygen reduction and hydrogen evolution reactions [J]. **ACS Catalysis**, 2016, **6**(2): 1045-1053.

[11] YANG Tianyu, ZHOU Ruifeng, WANG Dawei, *et al*. Hierarchical mesoporous yolk-shell structured carbonaceous nanospheres for high performance electrochemical capacitive energy storage [J]. **Chemical Communications**, 2015, **51**(13): 2518-2521.

[12] ZHOU Min, PU Fan, WANG Zhao, *et al*. Nitrogen-doped porous carbons through KOH activation with superior performance in supercapacitors [J]. **Carbon**, 2014, **68**: 185-194.

[13] DUAN Xiaoguang, AO Zhimin, ZHOU Li, *et al*. Occurrence of radical and nonradical pathways from carbocatalysts for aqueous and nonaqueous catalytic oxidation [J]. **Applied Catalysis B: Environmental**, 2016, **188**: 98-105.

[14] WANG Xiaobo, QIN Yanlei, ZHU Lihua, *et al*. Nitrogen-doped reduced graphene oxide as a bifunctional material for removing bisphenols:

synergistic effect between adsorption and catalysis [J]. **Environmental Science & Technology**, 2015, **49**(11): 6855-6864.

[15] DUAN X, O'DONNELL K, SUN H, *et al*. Sulfur and nitrogen Co-doped graphene for metal-free catalytic oxidation reactions [J]. **Small**, 2015, **11**(25): 3036-3044.

[16] KATTEL S, ATANASSOV P, KIEFER B. Catalytic activity of Co-N_x/C electrocatalysts for oxygen reduction reaction: a density functional theory study [J]. **Physical Chemistry Chemical Physics**, 2013, **15**(1): 148-153.

[17] AL-ANAZI A, ABDELRAHEEM W H, HAN C, *et al*. Cobalt ferrite nanoparticles with controlled composition-peroxymonosulfate mediated degradation of 2-phenylbenzimidazole-5-sulfonic acid [J]. **Applied Catalysis B: Environmental**, 2018, **221**: 266-279.

[18] FARHA O K, ERYAZICI I, JEONG N C, *et al*. Metal-organic framework materials with ultrahigh surface areas: is the sky the limit? [J]. **Journal of the American Chemical Society**, 2012, **134**(36): 15016-15021.

[19] ROWSELL J L C, YAGHI O M. Metal-organic frameworks: a new class of porous materials [J]. **Microporous and Mesoporous Materials**, 2004, **73**(1): 3-14.

[20] TANG H, CAI S, XIE S, *et al*. Metal-organic-framework-derived dual metal- and nitrogen-doped carbon as efficient and robust oxygen reduction reaction catalysts for microbial fuel cells [J]. **Advanced Science**, 2016, **3**(2): DOI:10.1002/advs.201500265.

[21] LAI Q, ZHU J, ZHAO Y, *et al*. MOF-based metal-doping-induced synthesis of hierarchical porous Cu-N/C oxygen reduction electrocatalysts for Zn-air batteries [J]. **Small**, 2017, **13**(30): DOI:10.1002/small.201700740.

[22] DUAN Xiaoguang, SUN Hongqi, WANG Yuxian, *et al*. N-doping-induced nonradical reaction on single-walled carbon nanotubes for catalytic phenol oxidation [J]. **ACS Catalysis**, 2015, **5**(2): 553-559.

[23] CHEN Yuzhen, WANG Chengming, WU Zhenyu, *et al*. From bimetallic metal-organic framework to porous carbon: high surface area and multicomponent active dopants for excellent electrocatalysis [J]. **Advanced Materials**, 2015, **27**(34): 5010-5016.

氮掺杂多孔碳包覆钴金属催化去除有机污染物

王冠龙, 毕晨曦, 陈 硕*, 全 燮, 于洪涛

(大连理工大学 工业生态与环境工程教育部重点实验室, 辽宁 大连 116024)

摘要: 活化过硫酸氢盐(PMS)产生具有强氧化能力的硫酸根自由基($SO_4^{\cdot-}$)的高级氧化技术在有机污染物降解方面正受到越来越多的关注.选择 ZIF-67 为前驱体通过两步热处理构建氮掺杂多孔碳包覆钴金属的核壳催化剂(Co@NPC),并通过改变碳化温度调控多孔碳壳的结构与组成,研究多孔碳结构组成对催化性能的影响.实验结果表明,随着碳化温度的升高,介孔孔容与碳壳厚度逐渐增大,催化剂的性能随着介孔孔容与碳壳厚度比值的增加而显著提高.850 ℃碳化的 Co@NPC 催化降解苯酚的动力学常数是多相催化剂四氧化三钴的 110.8 倍,甚至是之前报道过最优的 PMS 催化剂均相钴离子的 4.6 倍.此外,当包覆的碳层数大于 3 时,Co@NPC 表现出良好稳定性,钴溶出明显减少.碳壳的介孔孔容与厚度是影响 PMS 活化的重要因素,Co@NPC 的催化性能还受到石墨氮含量的影响.

关键词: 过硫酸氢盐(PMS);硫酸根自由基;氮掺杂多孔碳;核壳催化剂;苯酚降解

中图分类号: X505;O643.36 **文献标识码:** A **doi:** 10.7511/dllgxb201804001

收稿日期: 2017-12-10; **修回日期:** 2018-05-25.

基金项目: 国家自然科学基金资助项目(重大项目:21590813);高等学校学科创新引智计划资助项目(B13012).

作者简介: 王冠龙(1990-),男,博士,E-mail:stevewgl@mail.dlut.edu.cn;陈 硕*(1974-),女,博士,副教授,E-mail:shuochen@dlut.edu.cn.